RSC Advances

PAPER

View Article Online
View Journal | View Issue

Cite this: *RSC Adv.*, 2017, **7**, 23328

In situ growth of NiO nanoparticles on carbon paper as a cathode for rechargeable Li–O_2 batteries

Hong-qiang Wang,[ac] Xiao-ping Fan,[a] Xiao-hui Zhang,[a] You-guo Huang,[a] Qiang Wu,[b] Qi-chang Pan[a] and Qing-yu Li *[ab]

Received 10th March 2017
Accepted 24th April 2017

DOI: 10.1039/c7ra02932b

rsc.li/rsc-advances

Novel NiO nanoparticles have been successfully designed and directly grown on carbon paper (CP) as a cathode for rechargeable Li–O_2 batteries *via* a facile two-step *in situ* synthesis strategy, including a simple electro-deposition technique, following by high temperature oxidation. Using *in situ* synthesis methods means that the porous structure of CP is effectively inherited and the use of a binder avoided, which eliminates possible side reactions and over-potential from the binder and enhances the electrochemical performance. SEM and TEM show that the NiO nanoparticles homogenously cover the exposed surface of CPs and the size of the NiO particles is around 10 nm. Benefiting from these structural advantages, the binder-free cathode of NiO/CP exhibits a high discharge capacity of 8934 mA h g^{-1} under the current density of 100 mA g^{-1} and could cycle more than 112 times within a capacity limitation of 500 mA h g^{-1}.

Introduction

In recent years, the global energy crisis and environmental destruction situation are getting worse, and the development of efficient and clean energy sources has become imperative.[1] Owing to their significantly high theoretical specific energy density (5200 W h kg^{-1}), rechargeable Li–O_2 batteries (LOBs) are a kind of energy storage and conversion device that is a promising candidate for next-generation electric power sources.[2–5] The theoretical energy density of Li–O_2 batteries is about eight times higher than the conventional Li-ion batteries because of the fact that the cathode active material (oxygen) is obtained directly from the atmosphere without being stored in the batteries.[6,7] A typical nonaqueous Li–O_2 battery is composed of a Li metal anode in contact with a Li-ion containing organic electrolyte and a porous cathode.[8] During discharging, oxygen from the atmosphere combines with Li^+ to yield discharge products (*e.g.* Li_2O_2), which is defined as the oxygen reduction reaction (ORR). During charging, the discharge products decompose to Li^+ and oxygen, which is defined as the as the oxygen evolution reaction (OER).[7,9–11] Many efforts have been devoted to develop high performance Li–O_2 batteries. However, the development of Li–O_2 batteries is still in the initial stage, there are still many problems (such as low round-trip efficiency, instability of the batteries and especially poor cycle life) restricting the practical application of Li–O_2 batteries.[12–16]

In order to solve the above problems, developing a suitable catalyst is the critical link to achieve the application of Li–O_2 batteries. On the one hand, high performance catalyst can accelerate the ORR and OER as well as reducing the over-potential for Li–O_2 batteries, on the other hand, an active catalyst can effectively catalyze the decomposition of solid discharge products, which would improve cycle life and round-trip efficiency of Li–O_2 batteries.[17,18] In recent years, many efforts have been devoted to study transition metal oxide due to their advantages of low cost, excellent catalytic activity and natural abundance.[19–22] NiO has been studied in Li–O_2 battery due to its good catalytic performance,[23–26] Swapna Ganapathy also confirmed that Li_2O_2 was more easily formed on the surface of NiO owing to its potential nucleation site for the formation of Li_2O_2, and this is supported by first principle calculations, which predict a low interfacial energy for the formation of NiO–Li_2O_2 interfaces.[27]

However, the poor conductivity of NiO limits its electrochemical performance. To overcome this problem, one effective way to improve the conductivity of electrons is to add an electron-conductive material as a support for the catalyst. Meanwhile, such support should contain a lot of mesoporous to provide more void spaces for storing Li_2O_2. Carbon paper has been widely used as the collector of Li–O_2 batteries because of its unique porous structure and excellent electrical conductivity.[28–30]

Herein, we report a facile two-step procedure successfully load uniformly NiO nanoparticles on the carbon paper (NiO/CP). It is worth mentioning that this method was first proposed to prepare NiO nanoparticles catalyst for Li–O_2

[a]*School of Chemistry and Pharmaceutical Sciences, Guangxi Normal University, Guilin 541004, China. E-mail: liqingyu62@126.com*

[b]*Guangxi Key Laboratory of Low Carbon Energy Materials, School of Chemical and Pharmaceutical Sciences, Guangxi Normal University, Guilin 541004, China*

[c]*College of Chemical Engineering, Huanggang Normal University, Huanggang 438000, China*

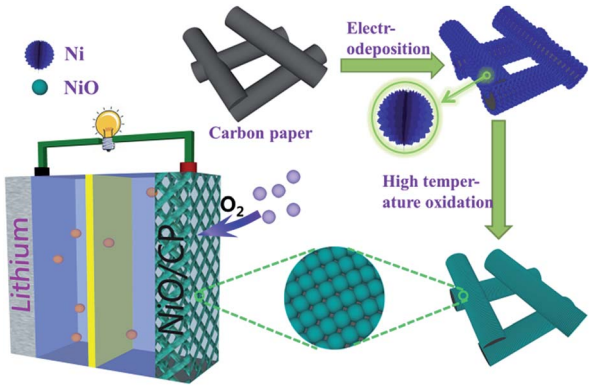

Fig. 1 Synthetic process of NiO/CP and structure of the rechargeable Li–O_2 batteries.

batteries. As shown in Fig. 1, firstly, we use an effective and simple electro-deposition method to prepare a free-standing material that Ni nano-flowers directly grown from carbon paper and then calcined oxidized to NiO at 550 °C in an air atmosphere. Using *in situ* synthesis methods synthesized NiO directly on the CPs to avoid the use of the binder, it eliminates the problem of great polarization and poor electrochemical performance due to the addition of the binder and inherits the porous structure of CPs that promotes rapid transmission of oxygen and Li ion and infiltration of electrolyte. In addition, using electro-deposition method can effectively control the morphology and size of the catalyst particles, increasing the active surface area of the catalyst to improve the utilization of the catalyst,[20] so that the electrochemical performance is improved greatly.

Experimental

Preparation of NiO/CP

The positive electrodes were prepared *via in situ* fabricate NiO nanoparticles anchored on carbon paper (NiO/CP). Firstly, we electrodeposited nickel metal particles on carbon paper (Ni/CP) under a current of 40 mA cm^{-2} deposition for 30 s wherein titanium plate as the anode, carbon paper as the cathode. The electro-deposition solutions consists of 100 g L^{-1} $NiSO_4 \cdot 6H_2O$, 60 g L^{-1} $NiCl_2 \cdot 6H_2O$, 40 g L^{-1} H_3BO_3, 0.1 g L^{-1} CN_2H_4S and 0.1 g L^{-1} $C_{12}H_{25}SO_3Na$. Then the samples were washed with deionized water and dried at 80 °C for 1 h. Finally, we put Ni/CP composite into the Branch Crystal tube furnace to calcine in air atmosphere, and kept at 550 °C for 2 h. As a result, the metal nickel oxidized to NiO.

Characterization of the electrodes

The morphology and structure of the NiO/CP are investigated by scanning electron microscopy (SEM, Philips, FEI Quanta 200 FEG) and transmission electron microscopy (TEM, JEOL 2011). The content of various components of NiO/CP composite was determined from thermogravimetric analysis (TGA) (Nitzsch STA 449C) at a heating rate of 5 °C min^{-1}. The phases present in the electrode were checked by X-ray diffraction (XRD-Rigaku D/Max-2550pc) with Cu Kα radiation (λ = 0.1541 nm). X-ray photoelectron spectroscopy (XPS) experiments were carried out using an AXIS ULTRA DLD instrument, using aluminum Kα X-ray radiation during the XPS analysis.

Electrode preparation and electrochemical measurements

Electrochemical characterizations of Li–O_2 cells were carried out using 2032-type coin cells which were assembled in an argon-filled glovebox. Li foil was used as the anode, 1 mol L^{-1} LiTFSi in mixed solution of tetraethylene glycol dimethyl ether (TEGDME) was used as the electrolyte, Celgard 2400 and a glass fiber were used as the separator and the NiO/CP composites as the cathode. The cells were sealed except holes of the cathode shell exposed to 1 atm O_2 environment. The electrochemical properties were studied with a Land batteries measurement system (LAND BT2013A, Wuhan, China). Galvanostatic charge–discharge cycling was performed over a voltage window of 2.2–4.3 V. The working electrode was measured at room temperature during the whole process.

Results and discussion

CPs, owning porous skeleton and stability, are popular current collectors for Li–O_2 batteries. The porous and interconnected morphology of CPs is shown in Fig. 2a. Because of its interconnected 3D scaffold structure which are benefit to the rapid transmission of oxygen and the contact with the electrolyte and the surface of catalyst, so it is used as a template for the growth of NiO. High magnification SEM of CPs indicates that CPs are consist of carbon fibers and the surface of CPs are smooth. From the Fig. 2c and d we can clearly see that the flower metal nickel were successfully coated on the surface of the CPs by electro-deposition method and the size of nickel particle is around 50 nm. The SEM images of the NiO/CP are shown in Fig. 2e–g. In contrast to Fig. 2a and e, we can clearly see that nickel oxide homogenously cover the exposed surface of CPs. From high-magnification SEM of NiO/CP we can clearly see the uniform and dense surface structure of NiO/CP and the diameter of the NiO particles sizes which is only about 10 nm in Fig. 2f and g. Nanoscale NiO particles improved the specific surface area of cathode materials and more active sites were exposed, thereby effectively improve the catalytic performance. The corresponding elemental mapping spectrum of the NiO/CP as shown in Fig. 2h, it can be seen that the carbon, oxygen and nickel elements are homogeneously distributed in the whole detected area and suggest that NiO nanoparticles were uniformly loaded on the carbon paper.

Transmission electron microscope (TEM) analysis was performed to further characterize the detailed morphology and microstructure of the NiO/CP electrode. As shown in Fig. 3a and b, TEM image indicates that NiO nanoparticles uniformly distributed on the carbon paper with an average size of 10 nm. High magnification TEM image of Fig. 3c reveals the spacing of the adjacent lattice planes is 0.24 nm corresponding to the (111) planes of NiO phase, which is further confirmed by X-ray diffraction (XRD) (space group: $Fm\bar{3}m$ (225), JCPDS no. 47-1049).

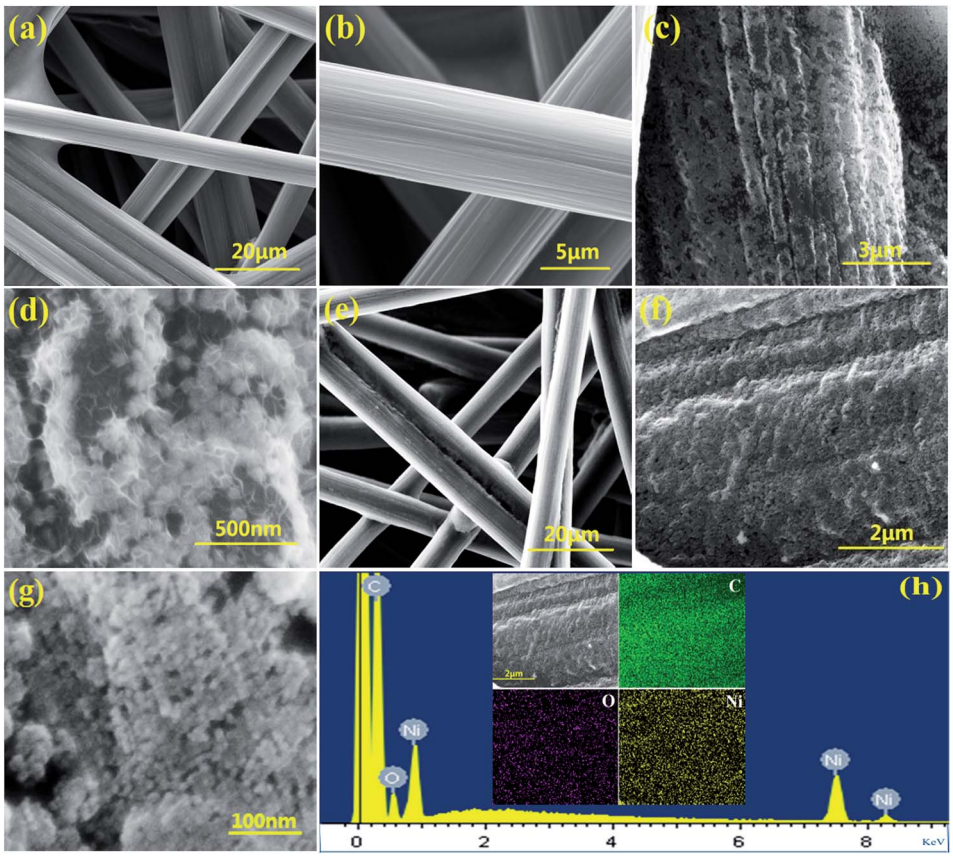

Fig. 2 (a and b) SEM image of pristine CP; (c and d) SEM of the Ni/CP composite; (e–g) SEM of the NiO/CP composite; (h) EDS of the C, O, Ni.

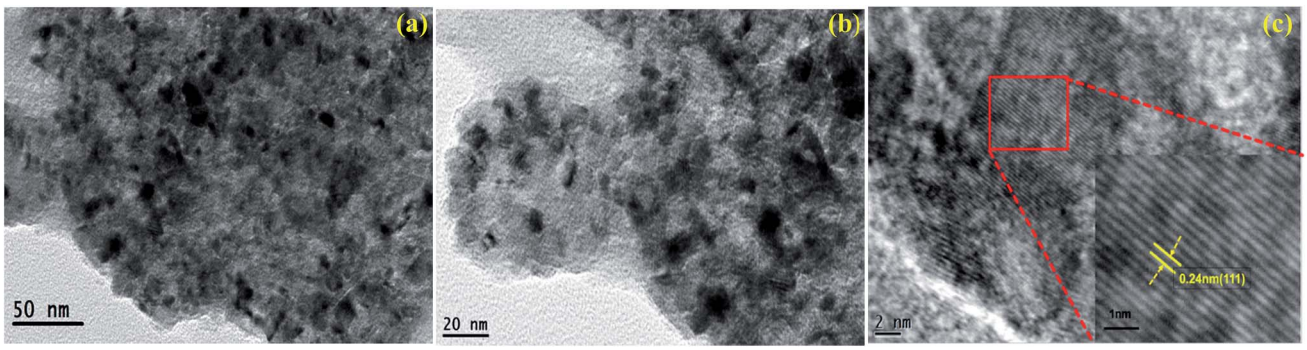

Fig. 3 (a–c) TEM images of NiO/CP.

The content of NiO in the NiO/CP composite was confirmed by the thermo-gravimetric analysis (TGA) in O_2. The TGA curves of the NiO/CP composite is shown in Fig. 4. The one continuous weight loss in the range of approximately 570–800 °C for the NiO/CP composite is attributed to the oxidation of C of carbon paper to CO_2, when the temperature is higher than 800 °C, the TGA curves tends to be gentle, indicating that the C element has all become CO_2. The mass fraction of NiO and CP in the NiO/CP composite can be calculated to be around 7.75% and 92.25%, respectively.

The XRD patterns of CP and the NiO/CP composites of with the electro-deposition time of 30 s and 300 s are shown in Fig. 5. The pure carbon paper shows one intense diffraction peaks located at 26.3° and one weak diffraction peaks at 54.2°. Compared with the pure carbon paper, when the electro-deposition time which is consistent with experimental conditions is 30 s, the NiO/CP composites with shows there was no significant change, which may be attributed to that the content of NiO is too little to detect and the disturbance of high intensity of the C peak. When increasing the deposition time to 300 s, the deposited quantity of NiO on carbon paper increases, which is obvious in the XRD pattern. The NiO/CP composites exhibits the typical characteristic peaks of NiO at 37.24°, 43.27° and 62.86°, according to JCPDS card no. 71-1179, these peaks can be

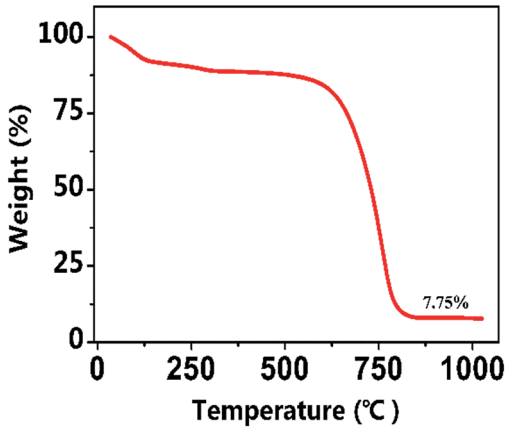

Fig. 4 TGA analysis for the NiO/CP composite.

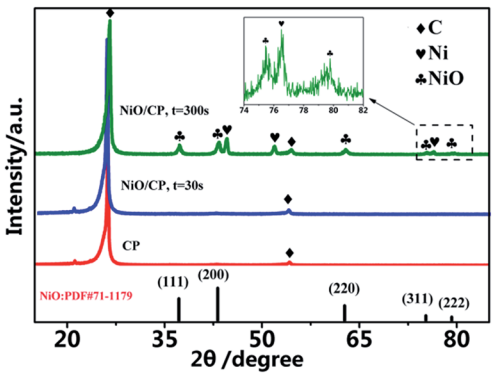

Fig. 5 The XRD patterns of CP and the NiO/CP composites of with the electro-deposition time of 30 s and 300 s.

assigned to the (111), (200) and (311) plane reflections of the NiO, respectively. Highlighted X-ray diffraction patterns related to the 2θ range of 19–23° are shown in Fig. 5, there are two low-intensity peaks at 75.39° and 79.38°, which can be attributed to the (311) and (222) plane reflections of the NiO, respectively. In addition, there are some Ni peaks in the XRD pattern due to incomplete oxidation of Ni.

The chemical states of NiO/CP is also confirmed by X-ray photoelectron spectroscopy (XPS) measurements. Fig. 6a shows the XPS survey scan of the NiO/CP, which indicates the presence of Ni, O, and C elements and shows a 2.76 at% percentage composition of Ni and this content is obviously lower than the detection range of XRD. Fig. 6b–d show the Ni 2p, O 1s and C 1s peaks, which were analyzed by using the software of XPS peak version 4.1. In the Ni 2p spectra of Fig. 6b, the main Ni $2p_{3/2}$ peak located at 861.4 eV, 855.2 eV and 851.1 eV (ref. 31 and 32) which all are characteristic peaks of the NiO and located at 861.7 eV which is characteristic peak of the $Ni(OH)_2$.[33] As shown in Fig. 6c, three peaks for the O 1s are observed at 529.5 eV, 531.2 eV and 532.4 eV, which are associated with O 1s binding energy in O–Ni, Ni–O–H and O–C,[34,35] respectively. In the C 1s spectra of Fig. 6d indicates that NiO/CP has three peaks at 284.6 eV, 284.7 eV and 285.6 eV, which

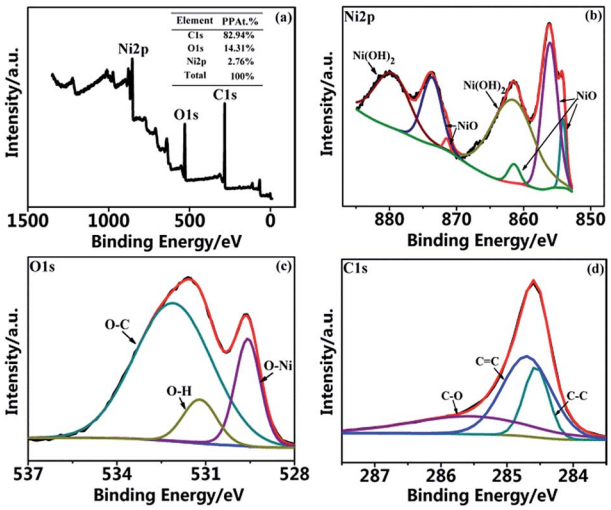

Fig. 6 XPS spectra of the NiO/CP composite. (a) Survey scan; (b) Ni 2p spectrum; (c) O 1s spectrum; (d) C 1s spectrum.

correspond to the binding energies of C 1s in C–C, C=C and C–O, respectively.[20]

The electrochemical performance of the as-prepared NiO/CP was investigated by the galvanostatic discharge/charge method. Fig. 7a and b shows the charge and discharge curves obtained by limiting the capacity of 1000 mA h g^{-1} at various current density. It can be observed from Fig. 7a that there is a very small overpotential of 0.55 V in the middle of the charge–discharge plateaus at the current density of 100 mA g^{-1}. As the current densities increasing, the overpotential increases appropriately, when the current density increased to 300 mA g^{-1}, the overpotential increases to 1.3 V, but is still smaller than the overpotential of the general Li–O_2 batteries. Besides, Fig. 7b shows the discharge curves of the Li–O_2 batteries with the NiO/CP electrode at different current densities. At 100 mA g^{-1}, the batteries deliveres extremely high discharge specific capacity of 8934.0 mA h g^{-1}, when the current density were increased to 200 mA g^{-1} and 300 mA g^{-1}, the batteries still show higher discharge specific capacity of 5000.4 mA h g^{-1} and 4361.4 mA h g^{-1}, respectively, exhibiting good rate capability of the Li–O_2 batteries with the NiO/CP electrode. The full discharge–charge curves of the first ten cycles of the Li–O_2 batteries with the NiO/CP electrode at the current density of 100 mA g^{-1} as shown in Fig. 7c. The first discharge specific capacity of the Li–O_2 batteries is up to 8934.0 mA h g^{-1} with a discharge platform of 2.73 V. Comparing with other Li–O_2 batteries systems which using NiO as catalyst, it exhibits the highest discharge specific capacity, which may be due to its unique spherical nanoparticles and allowing more active sites to be exposed.[23–26] After 5 cycles, the discharge specific capacity is still higher 4000 mA h g^{-1}, while after 10 cycles, the discharge specific capacity decreased to 1327 mA h g^{-1}. In fact, the stable full discharge/charge Li–O_2 batteries system still can't be achieved due to the accumulation of the discharge product and instability of the electrolyte, which is still a serious challenge to be solved for Li–O_2 batteries. The excellent electrochemical performance NiO/CP

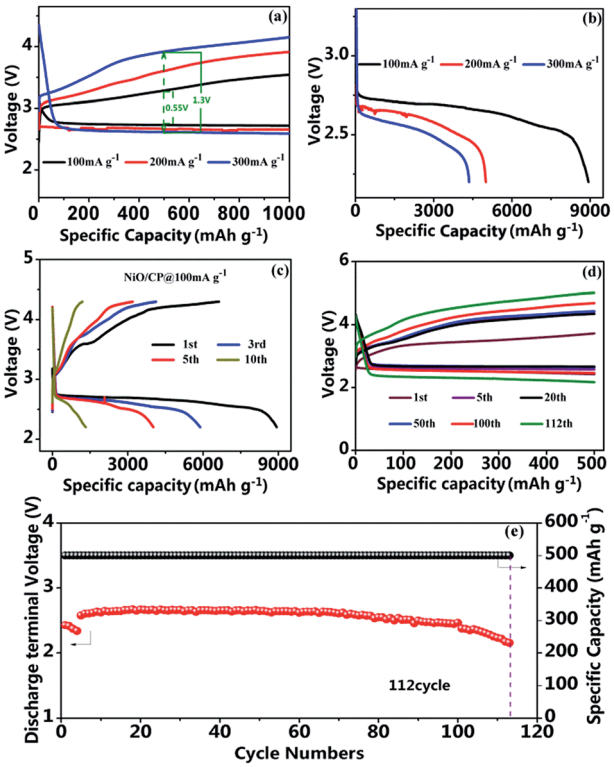

Fig. 7 Electrochemical properties of NiO/CP catalyzed Li–O_2 batteries. (a) Discharge/charge curves of Li–O_2 batteries with NiO/CP electrodes at the current density of 100 mA g^{-1}, 200 mA g^{-1} and 300 mA g^{-1} with a limited of 1000 mA h g^{-1} based on mass of NiO; (b) the rate capacities of Li–O_2 batteries using NiO/CP electrode at the current density of 100 mA g^{-1}, 200 mA g^{-1} and 300 mA g^{-1}; (c) full discharge/charge curves between 2.2–4.3 V at 100 mA g^{-1}; (d) cycling performance of NiO/CP electrodes at 100 mA g^{-1} with limited capacity of 500 mA h g^{-1}; (e) capacity and terminal voltage of discharge *vs.* cycle numbers.

electrode is due to unique three dimensional structure, high catalytic activity of NiO nanoparticles. As shown in Fig. 7d and e, the cycle stability of NiO/CP cathode is investigated with a an upper-limit capacity to 500 mA h g^{-1} at a current density of 100 mA g^{-1} based on mass of NiO in the range of 2.0–5.0 V *versus* Li/Li^+. Fig. 7d displays the superior cycle performance and excellent stability of the LOBs with NiO/CP electrode which can be cycled for 112 cycles and most of the discharge capacities are delivered above 2.6 V. The 1st, 5th, 20th, 50th, 100th and 112th cycles of discharge/charge voltage profiles are selected to display in Fig. 7e, which further validated the excellent catalytic performance of NiO/CP composites.

In order to further demonstrate the catalytic properties of NiO, we made a comparison with pristine CP. NiO/CP and CP were used as cathode and were assembled into the LOBs to compare their electrochemical performance, which the specific capacity was calculated based on the total mass of the whole cathode electrode. As shown in Fig. 8, the Li–O_2 batteries with the NiO/CP cathode and pristine CP electrode without NiO were cycled at the current density of 0.05 mA cm^{-2}. The initial discharge capacity of the NiO/CP cathode is 12.4 mA h g^{-1}, after 5th cycles, the capacity reduced to 8.0 mA h g^{-1} and has been remained around 8.0 mA h

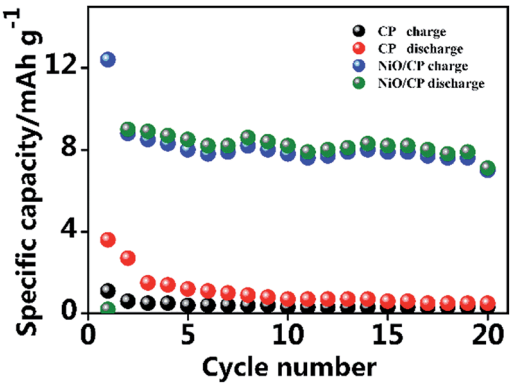

Fig. 8 Discharge/charge cycling of Li–O_2 cell with the NiO/CP cathode and pure CP electrode without NiO, based on total electrode mass at a current density of 0.05 mA cm^{-2}.

g^{-1} until to 20th cycles. As a comparison, the initial discharge capacity of the pristine CP cathode is only 3.6 mA h g^{-1}, after 5th cycles, the capacity reduced to 1.2 mA h g^{-1} and after 20th cycles, the capacity is only 0.5 mA h g^{-1}. Compared with the pure CP without NiO, the NiO/CP composite has greatly improved the specific capacity of Li–O_2 batteries.

Conclusions

In summary, we have designed a novel NiO nanoparticles directly grown on carbon paper *via* an *in situ* method as the cathode for Li–O_2 batteries. Compared with other methods, the size of NiO nanoparticle obtained by this method is far less than hexagonal plate NiO, so the specific surface area of NiO were greatly improved and more active site were exposed. In addition, this strategy can make NiO only deposit on surface of CPs, thus the NiO/CP electrode inheriting the porous structure of CPs that promotes rapid transmission of oxygen and infiltration of electrolyte. SEM and TEM show that the NiO nanoparticles homogenously cover the surface of CPs and the size of the NiO particles is around 10 nm. Benefiting from the structural advantages, the binder-free cathode of NiO/CP exhibits excellent catalytic performance and delivers high discharge capacity of 8934 mA h g^{-1} under the current density of 100 mA g^{-1} and could cycle more than 112 times within a capacity limitation of 500 mA h g^{-1}. These results suggest that NiO/CP composite as binder-free and freestanding cathode electrocatalyst, which exhibits good electrochemical performance would promote the practical application of LOBs.

Acknowledgements

This research was supported by National Science Foundation of China (U1401246, 51364004, 51474077, 21473042 and 51474110), Guangxi Natural Science Foundation (2012GXNSFAA053214).

Notes and references

1 B. Dunn, H. Kamath and J. M. Tarascon, *Science*, 2011, **334**, 928–935.

2 P. G. Bruce, S. A. Freunberger, L. J. Hardwick and J. M. Tarascon, *Nat. Mater.*, 2012, **11**, 19–29.
3 L. Grande, E. Paillard, J. Hassoun, J. B. Park, Y. J. Lee, Y. K. Sun, S. Passerini and B. Scrosati, *Adv. Mater.*, 2015, **27**, 784–800.
4 R. Black, B. Adams and L. F. Nazar, *Adv. Energy Mater.*, 2012, **2**, 801–815.
5 Y. Shao, F. Ding, J. Xiao, J. Zhang, W. Xu, S. Park, J.-G. Zhang, Y. Wang and J. Liu, *Adv. Funct. Mater.*, 2013, **23**, 987–1004.
6 G. A. Elia, J. Hassoun, W. J. Kwak, Y. K. Sun, B. Scrosati, F. Mueller, D. Bresser, S. Passerini, P. Oberhumer, N. Tsiouvaras and J. Reiter, *Nano Lett.*, 2014, **14**, 6572–6577.
7 Z. Peng, S. A. Freunberger, Y. Chen and P. G. Bruce, *Science*, 2012, **337**, 563–566.
8 Z. Ma, X. Yuan, L. Li, Z.-F. Ma, D. P. Wilkinson, L. Zhang and J. Zhang, *Energy Environ. Sci.*, 2015, **8**, 2144–2198.
9 K. Abraham and Z. Jiang, *J. Electrochem. Soc.*, 1996, **143**, 1–5.
10 Y. Yang, T. Zhang, X. Wang, L. Chen, N. Wu, W. Liu, H. Lu, L. Xiao, L. Fu and L. Zhuang, *ACS Appl. Mater. Interfaces*, 2016, **8**, 21350–21357.
11 T. Ogasawara, A. Débart, M. Holzapfel, P. Novák and P. G. Bruce, *J. Am. Chem. Soc.*, 2016, **128**, 1390–1393.
12 Y. Jing and Z. Zhou, *ACS Catal.*, 2015, **5**, 4309–4317.
13 P. Zhang, R. Wang, M. He, J. Lang, S. Xu and X. Yan, *Adv. Funct. Mater.*, 2016, **26**, 1354–1364.
14 S.-M. Xu, Q.-C. Zhu, J. Long, H.-H. Wang, X.-F. Xie, K.-X. Wang and J.-S. Chen, *Adv. Funct. Mater.*, 2016, **26**, 1365–1374.
15 Q. C. Liu, J. J. Xu, D. Xu and X. B. Zhang, *Nat. Commun.*, 2015, **6**, 7892.
16 C. Zhao, C. Yu, S. Liu, J. Yang, X. Fan, H. Huang and J. Qiu, *Adv. Funct. Mater.*, 2015, **25**, 6913–6920.
17 D. Geng, N. Ding, T. S. A. Hor, S. W. Chien, Z. Liu, D. Wuu, X. Sun and Y. Zong, *Adv. Energy Mater.*, 2016, **6**, 1502164.
18 Z. Huang, B. Chi, L. Jian, S. Youyi and Y. Liu, *J. Alloys Compd.*, 2017, **695**, 3435–3444.
19 W. H. Ryu, T. H. Yoon, S. H. Song, S. Jeon, Y. J. Park and I. D. Kim, *Nano Lett.*, 2013, **13**, 4190–4197.
20 H.-Q. Wang, J. Chen, S.-J. Hu, X.-H. Zhang, X.-P. Fan, J. Du, Y.-G. Huang and Q.-Y. Li, *RSC Adv.*, 2015, **5**, 72495–72499.
21 J. Liu, R. Younesi, T. Gustafsson, K. Edström and J. Zhu, *Nano Energy*, 2014, **10**, 19–27.
22 L. Jin, L. Xu, C. Morein, C.-h. Chen, M. Lai, S. Dharmarathna, A. Dobley and S. L. Suib, *Adv. Funct. Mater.*, 2010, **20**, 3373–3382.
23 D. Qiu, G. Bu, B. Zhao, Z. Lin, L. Pu, L. Pan and Y. Shi, *Mater. Lett.*, 2015, **141**, 43–46.
24 S. Tong, M. Zheng, Y. Lu, Z. Lin, J. Li, X. Zhang, Y. Shi, P. He and H. Zhou, *J. Mater. Chem. A*, 2015, **3**, 16177–16182.
25 M. Hong, H. C. Choi and H. R. Byon, *Chem. Mater.*, 2015, **27**, 2234–2241.
26 C. Wang, Y. Zhao, J. Liu, P. Gong, X. Li, Y. Zhao, G. Yue and Z. Zhou, *Chem. Commun.*, 2016, **52**, 11772–11774.
27 S. Ganapathy, Z. Li, M. S. Anastasaki, S. Basak, X. F. Miao, K. Goubitz, H. W. Zandbergen, F. M. Mulder and M. Wagemaker, *J. Phys. Chem. C*, 2016, **120**, 18421–18427.
28 Z. Guo, G. Zhu, Z. Qiu, Y. Wang and Y. Xia, *Electrochem. Commun.*, 2012, **25**, 26–29.
29 J. Yi, K. Liao, C. Zhang, T. Zhang, F. Li and H. Zhou, *ACS Appl. Mater. Interfaces*, 2015, **7**, 10823–10827.
30 Y.-g. Huang, J. Chen, X.-h. Zhang, Y.-h. Zan, X.-m. Wu, Z.-q. He, H.-q. Wang and Q.-y. Li, *Chem. Eng. J.*, 2016, **296**, 28–34.
31 A. N. Mansour, *Surf. Sci. Spectra*, 1994, **3**, 239–246.
32 S. Uhlenbrock, C. Scharfschwerdt, M. Neumann, G. Illing and H. Freund, *J. Phys.: Condens. Matter*, 1992, **4**, 7973.
33 A. N. Mansour and C. A. Melendres, *Surf. Sci. Spectra*, 1996, **3**, 247–254.
34 L. C. Lopez, D. W. Dwight and M. B. Polk, *Surf. Interface Anal.*, 1986, **9**, 405–409.
35 J. Haber, J. Stoch, L. Ungier, J. Haber, J. Stoch and L. Ungier, *J. Electron Spectrosc. Relat. Phenom.*, 1976, **9**, 459–467.